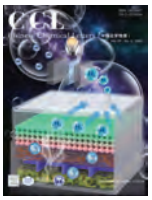
Chinese Chemical Letters 37 (2026) 111317

Contents lists available at ScienceDirect

Chinese Chemical Letters

journal homepage: www.elsevier.com/locate/cclet



Heptamethine cyanine with 1239 nm fluorescence emission for *in vivo* imaging

Junxiu Zhao[a], Jingya Shi[a], Xiaoli Sun[b], Siyu Wang[a], Xuwei Han[c], Xiaoni Zhao[c,*], Jisheng Nie[a,*], Yongkang Yue[c,*]

[a] *Key Laboratory of Coal Environmental Pathogenicity and Prevention, Ministry of Education, Shanxi Medical University, Taiyuan 030001, China*
[b] *Rushan Suboffice of Weihai Municipal Ecology and Environment Bureau, Rushan 264500, China*
[c] *Key Laboratory of Chemical Biology and Molecular Engineering of Ministry of Education, Institute of Molecular Science, Shanxi University, Taiyuan 030006, China*

ARTICLE INFO

Article history:
Received 26 February 2025
Revised 28 April 2025
Accepted 14 May 2025
Available online 15 May 2025

Keywords:
NIR-II
Fluorescent dyes
Heptamethine cyanine
Cyanine limit
In vivo imaging

ABSTRACT

Long-wavelength fluorescent dyes have revolutionized *in vivo* fluorescence imaging by offering unparalleled spatial resolution. Nevertheless, the majority of organic fluorescent dyes documented to date exhibit emission wavelengths predominantly within the range of 1000–1100 nm, with scarcely any surpassing the 1200 nm threshold. Herein, we introduce a heptamethine cyanine dye that boasts a remarkable fluorescence wavelength of 1239 nm. To our knowledge, this represents the longest fluorescence wavelength for heptamethine benzindole derivative. We have meticulously analyzed its photophysical characteristics and solvatochromic behavior, and assessed its efficacy *in vivo* fluorescence imaging applications.

© 2026 Published by Elsevier B.V. on behalf of Chinese Chemical Society and Institute of Materia Medica, Chinese Academy of Medical Sciences.

In recent years, with the widespread application of *in vivo* fluorescence imaging technology in the second near-infrared window (NIR-II, fluorescence wavelength range of 900–1700 nm) in scientific research, the results of *in vivo* fluorescence imaging based on this wavelength range have continuously redefined our understanding of the spatiotemporal resolution of fluorescence *in vivo* labelling [1–3]. This has significantly bolstered confidence in the practical application of fluorescence imaging technology *in vivo* [4,5]. For instance, *in vivo* fluorescence imaging with wavelengths exceeding 1200 nm, tissue autofluorescence drastically decreases, and light scattering by tissues for long-wavelength fluorescence is also significantly reduced, allowing us to distinguish between femoral arteries and veins at a micron-level resolution [6,7]. Moreover, this high signal-to-noise ratio imaging modality enables us to perform *in vivo* imaging of mice at millisecond temporal resolution, facilitating the analysis of physiological behaviours such as heart rate, respiration, and intestinal peristalsis through fluorescence imaging [8,9].

Since their first report in 1856, cyanines have been a predominant class of near-infrared fluorescent dyes [10]. The diversity and modifiability of their structures have secured their significant role in applications such as photodynamic therapy, photothermal therapy, and *in vivo* fluorescence labelling [11,12]. Typically, the absorption and emission wavelengths of cyanines follow the vinylene shift rule, where each additional pair in the polymethine chain results in a wavelength extension of approximately 100 nm [13]. Additionally, cyanines exhibit a high molar extinction coefficient, ranking among the highest of existing fluorescent dyes. For dyes, the continuous redshift of fluorescence wavelengths inevitably leads to increased internal conversion, thereby limiting the fluorescence quantum yield [10]. Actually, for fluorescent dyes with peak wavelengths above 1000 nm, the highest fluorescence quantum yield in low-polarity, low-viscosity solvents such as DCM is merely 0.5% [14]. Therefore, to ensure sufficient fluorescence brightness for *in vivo* imaging, the molar extinction coefficient becomes particularly crucial, which is one of the reasons cyanine dyes continue to attract widespread attention [15,16]. To date, commercially available cyanines with fluorescence peaks exceeding 1000 nm include Flav7, IR-26, IR-1061 and FD-1080 [17]. Furthermore, expanding the conjugated system brought continuous breakthroughs in the wavelength of cyanine derivatives. For instance, HC series dyes have demonstrated significant progress in extending the fluorescence emission wavelength, achieving a peak at 1376 nm [18]. In fact, despite these advancements, fluorescent

* Corresponding authors.
E-mail addresses: zhaoxiaoni@sxu.edu.cn (X. Zhao), niejisheng@sxmu.edu.cn (J. Nie), ykyue@sxu.edu.cn (Y. Yue).

https://doi.org/10.1016/j.cclet.2025.111317
1001-8417/© 2026 Published by Elsevier B.V. on behalf of Chinese Chemical Society and Institute of Materia Medica, Chinese Academy of Medical Sciences.

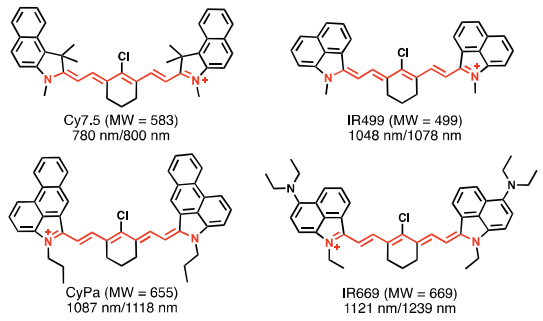


Fig. 1. Structural revolution of heptamethine cyanine with red-shifted fluorescence. The absorption and fluorescence wavelengths and the corresponding molecular weight of the dyes were labelled.

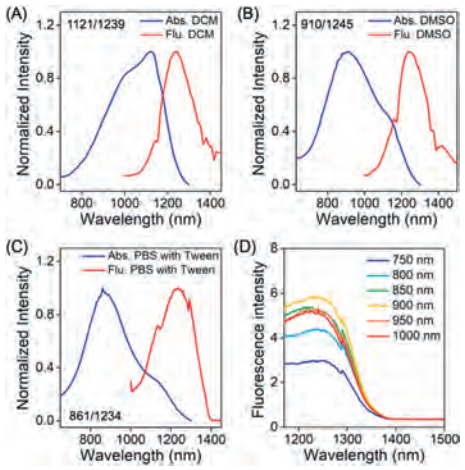


Fig. 2. Absorption and fluorescence spectra of IR-669 in DCM (A), DMSO (B) and PBS with Tween (C). The corresponding wavelengths were labelled in the figures. (D) Fluorescence spectra of IR-669 in DMSO upon various excitations.

dyes with emission peaks exceeding 1200 nm are scarce, and there is an urgent need for the development of dyes that combine structural rigidity with reliable synthesis and separation.

However, the aforementioned vinylogous extension strategy cannot indefinitely extend the absorption and fluorescence wavelengths of cyanine dyes due to the cyanine limit [19,20]. When the polymethine chain extends to 11 units, the long-wavelength, narrow absorption characteristics of cyanines may completely disappear [21–23]. Correspondingly, continuously expanding the conjugated structures at the termini of the polymethine chain prove to have minimal impact on extending the absorption and fluorescence wavelengths and significantly exacerbates dye aggregation, leading to fluorescence quenching [24,25]. Therefore, to address these challenges and mitigate the aggregation risks posed by overly expansive terminal group, while simultaneously extending the dye's absorption and emission wavelengths, we incorporated diethylamine into the benzindole moiety of a heptamethine backbone. The increased electron density lowers the energy gap between the ground and excited states and results in a redshift of the absorption and emission spectra. The obtained dye exhibited a peak fluorescence wavelength of 1239 nm, which is the longest fluorescence wavelength of the heptamethine benzindole derivative to date (Fig. 1). We characterized the structure and photophysical properties of this dye systematically and validated its real-time imaging performance *in vivo*.

The fluorescent dye was prepared through a 7-step synthesis. The relative molecular mass is 669, and in comparison to other reported dyes with similar fluorescence emission wavelengths, it holds an absolute advantage in terms of fluorescence wavelength/molecular mass. The specific structures, fluorescence wavelengths, and the corresponding fluorescence brightness data are listed in Table S1 (Supporting information). Therefore, considering atom economy and biological toxicity, this fluorescent dye has better potential for bioimaging applications. We named this fluorescent dye as IR-669. The absorption and fluorescence emission wavelengths of IR-669 in DCM are 1121 nm and 1239 nm (Fig. 2A), respectively, with a molar extinction coefficient and fluorescence quantum yield of 8.8×10^4 L mol^{-1} cm^{-1} (Fig. S1 Supporting information) and 0.091 % (IR1048 with 0.004 in DCM as the reference [26]), respectively. Its absorption spectrum exhibits typical cyanine characteristics, namely a main peak and a shoulder peak. In the highly polar DMSO solution, the absorption and fluorescence emission wavelengths of IR-669 shift to 910 nm and 1243 nm, respectively (Fig. 2B). The blue shift in its absorption spectrum is mainly due to the cation localization transformation caused by the solvent cage effect [22], a similar spectral change observed in the 11-methine cyanine dyes developed by Anderson's team [21]. Interestingly, we tested the ^{1}H NMR spectrum of IR-669 in DMSO, and the results showed that the dye exhibited high symmetry, which also implied that the reduction in electronic structure symmetry of the cyanine dye is not sufficient to be manifested in the NMR spectrum. Additionally, IR-669 undergoes fluorescence quenching in PBS solution, mainly due to the aggregation of the dye in water. In contrast, in PBS solution containing Tween, the absorption and fluorescence emission wavelengths of IR-669 are 861 nm and 1234 nm, respectively (Fig. 2C). As a derivative of IR-669, we also synthesized a near-infrared fluorescent dye IR-499 without dimethylamino modification. Similar to IR-669, IR-499 exhibits strict cyanine dye characteristics in DCM, with its absorption and fluorescence spectra maintaining a good mirror-image relationship, indicating the consistency of the dye's structure in the ground and excited states (Fig. S2 in Supporting information). This result is also preserved in the highly polar DMSO solution. The variation in the absorption wavelength of IR-669 in different solvents suggests that the increase in electronic density of the heptamethine dye exacerbates the sensitivity of the cyanine limit to solvent polarity.

The cyanine limit theory posits that cyanine dyes will transition from the uniform bond length characteristics of the methine skeleton to a polyethylene structure with alternating single and double bonds, resulting in a blue shift in the absorption spectrum. In previous research, crystal data were typically used to evaluate the bond length variation of the methine skeleton [21–23]. Presently, the spectral changes of IR-669 in different solvents suggest that experimental analysis of the cyanine limit in the solution may be possible. Therefore, we tested the Raman spectra of IR-669 in three solvent systems: DCM/DMSO (1/1, v/v), DMSO, and DMSO/water (1/1, v/v). The addition of DMSO to DCM was primarily to avoid the effects of temperature changes under laser irradiation. As shown in Fig. 3, the Raman signals of IR-669 in the three solvent systems are similar, with multiple scattering bands at 800, 1067, 1152–1180, 1346–1436, 1566, and 1623 cm^{-1}. Specifically, the 800 cm^{-1} signal is attributed to the stretching vibration of the C–Cl bond; the 1346–1436 cm^{-1} signal is dominated by the motion of the methine skeleton; and the 1566 cm^{-1} and 1623 cm^{-1} signals are mainly due to the stretching vibrations of the C=N bond [27–29]. As a representative polymethine derivative, symmetric oligoenes exhibit simplified Raman spectra in the 1300–1400 cm^{-1} band, a marker region for the vinylene spacer [30]. In contrast, asymmetric substitution disrupts molecular symmetry, leading to Raman band multiplication as the number of vinylene units increases [31]. A similar result was also observed in the merocyanines derivatives reported by the Garín group [32]. In our work, we observed that the 1346–1436 cm^{-1} signal undergoes increased splitting with increasing solvent polarity,

from a triplet signal in the DCM/DMSO system to a quintet signal in the DMSO and DMSO/water systems, directly indicating a decrease in the uniformity of the methine skeleton bond lengths. To our knowledge, this is the first experimental verification of the cyanine limit analysis of cyanine dyes in solution systems.

Interestingly, similar to the series of asymmetric cyanine dyes we previously reported, despite the significant blue shift in the absorption wavelength due to cation localization, the fluorescence emission wavelength remains largely consistent, primarily determined by the length of the methine skeleton and the size of the end-group conjugation system of the cyanine dye [33]. The theoretical explanation for this phenomenon is controversial, generally believed to be due to the excited state relaxation of the cyanine dye leading to the lowest vibrational level of the first excited state with uniform bond lengths, followed by a radiative transition back to the ground state. We validated this in the DMSO solvent system, observing that the fluorescence intensity of the system reaches its maximum value under 900 nm excitation as the excitation wavelength changes from 750 nm to 1000 nm (Fig. 2D). This result is consistent with the absorption spectrum of IR-669 in DMSO, further supporting the above theoretical understanding. In fact, although the cyanine limit has a minor effect on the fluorescence wavelength, the molar extinction coefficient of the dye will significantly decrease, for instance, the absorbance of IR-669 in DMSO is only 67 % of that in DCM. Therefore, in the structural modification of cyanine dyes, the cyanine limit is crucial for ensuring the brightness of the fluorescent dye.

We performed computational chemistry analysis on IR-669 and IR-499 at B3LYP/6–311+G(d) level using Gaussian 16 software with DCM as the solvent [34,35]. The corresponding frontier molecular orbitals and energy levels were presented in Fig. S3 (Supporting information). The calculated absorption and emission wavelengths of IR-669 and IR-499 were in excellent agreement with experimental results, confirming the reliability of the current theoretical basis set. Compared to IR-499, the symmetric introduction of the diethylamino moiety in IR-669 elevated the HOMO energy levels in both the Franck-Condon and locally excited states, resulting in a smaller HOMO-LUMO gap and thus longer absorption and emission wavelengths. For IR-669, the distribution of both HOMO and LUMO were primarily localized on the conjugation system (Fig. 3B). The distribution overlap indicated a localized excitation of IR-669 with significant $\pi \rightarrow \pi^*$ characteristic. This result was further supported by the corresponding oscillator strength of 2.52, represents

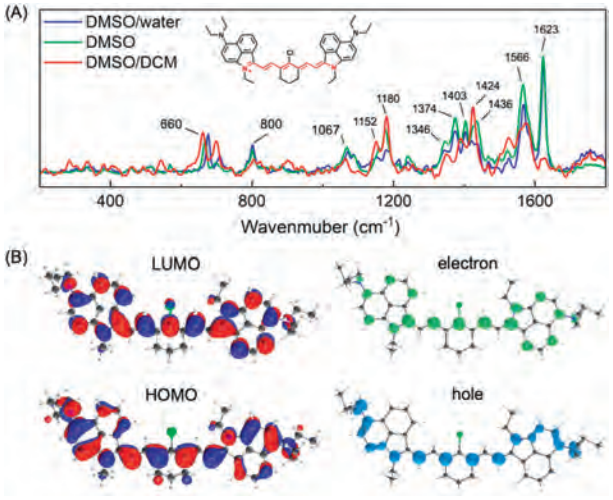


Fig. 3. (A) Raman spectrum and (B) computational calculation of IR-669. The mixed solvent means the volume ratio of 1/1. The electron-hole analysis was performed by Multiwfn. The visualization was generated by VMD.

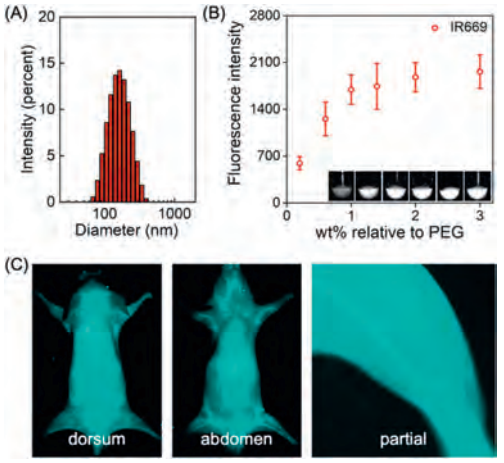


Fig. 4. Nanoparticles construction and the *in vivo* fluorescence imaging. (A) DLS data of the nanoparticles. (B) Dye proportion related fluorescence intensity evaluation. (C) *In vivo* fluorescence imaging upon IV injection of the nanoparticles. 808 nm laser with a power density of 100 mW/cm^2. A 1250 nm long-pass filter was used for the emission channel.

a high molar extinction coefficient. Based on electron-hole analysis, we determined that IR-669 exhibited minimal charge transfer characteristics during vertical excitation (Sr index of 0.728 a.u.) [36,37].

Due to the sensitivity of IR-669′s fluorescence activity to the solvent system, we encapsulated it in Methyl-PEG2000-DSPE to form nanoparticles and tested its potential for *in vivo* fluorescence imaging. To maximize its fluorescence performance, we first evaluated the mass ratio of IR-669 to the micelles. As shown in Fig. 4B, the fluorescence intensity of the nanoparticle in aqueous solution peaked at approximately 1 %, with a corresponding particle size of about 163 nm (Fig. 4A). The absorption and emission spectra of the nanoparticles were presented in Fig. S4 (Supporting information). Based on the cytotoxicity results (Fig. S5 in Supporting information), we performed real time *in vivo* fluorescence imaging experiments. After intravenous injection, the nanoparticles circulated in the blood and gradually accumulated in the liver which further metabolized *via* the hepatobiliary system (Fig. S6 in Supporting information). Imaging results showed that the dye could clearly image subcutaneous capillaries with high signal-to-noise ratio. In the imaging results of the inner thigh, the nanoparticles could be used for *in vivo* imaging of the femoral artery and vein with a signal-background-ratio of 1.78 (Fig. S7 Supporting information). In this work, the *in vivo* injection dose of the dye was only 0.24 mg/kg, significantly lower than that in other studies [38,39], ensuring imaging quality while minimizing the potential *in vivo* toxicity of the dye.

In this study, we present the structural optimization of a heptamethine cyanine dye tailored for the NIR-II window, culminating in the synthesis of a dye with a fluorescence peak at 1239 nm. A thorough assessment of the dye's photophysical properties and solvatochromic effects was undertaken, complemented by Raman spectroscopy to elucidate its structural nuances that straddle the cyanine limit. The dye's efficacy for *in vivo* imaging was corroborated at the organismal level. Our findings offer strategic insights into the wavelength extension and fluorescence intensity optimization of methine-based dyes.

Declaration of competing interest

The authors declare that they have no known competing financial interests or personal relationships that could have appeared to influence the work reported in this paper.

CRediT authorship contribution statement

Junxiu Zhao: Investigation. **Jingya Shi:** Investigation. **Xiaoli Sun:** Investigation, Data curation. **Siyu Wang:** Investigation. **Xuwei Han:** Investigation. **Xiaoni Zhao:** Investigation. **Jisheng Nie:** Investigation. **Yongkang Yue:** Supervision.

Acknowledgments

The work was supported by the National Natural Science Foundation of China (No. 22277069), Fundamental Research Program of Shanxi Province (Nos. 202303021222134; 202303021224003), Open Project Fund from Key Laboratory of Coal Environmental Pathogenicity and Prevention (Shanxi Medical University), Ministry of Education, China (No. MEKLCEPP/SXMU-202414), Doctor Fund Project of Shanxi Province (No. SD2324), and Doctor Fund Project of Shanxi Medical University (No. XD2222).

Supplementary materials

Supplementary material associated with this article can be found, in the online version, at doi:10.1016/j.cclet.2025.111317.

References

[1] F. Wang, Y. Zhong, O. Bruns, Y. Liang, H. Dai, Nat. Photonics 18 (2024) 535–547.
[2] J. Mu, M. Xiao, Y. Shi, et al., Angew. Chem. Int. Ed. 61 (2022) e202114722.
[3] Y. Chen, S. Wang, F. Zhang, Nat. Rev. Bioeng. 1 (2023) 60–78.
[4] Z. Chen, Y. Zhou, L. Li, et al., Small (2024) 2411787.
[5] X. Hu, Z. Fang, C. Zhu, et al., Adv. Funct. Mater. 34 (2024) 2401325.
[6] G. Hong, A.L. Antaris, H. Dai, Nat. Biomed. Eng. 1 (2017) 0010.
[7] F. Ding, Y. Fan, Y. Sun, F. Zhang, Adv. Heal. Mater. 8 (2019) 1900260.
[8] L. Wang, N. Li, W. Wang, et al., ACS Nano 18 (2024) 4683–4703.
[9] X. Hu, C. Zhu, F. Sun, et al., Adv. Mater. 36 (2023) 2304848.
[10] A. Mishra, R.K. Behera, P.K. Behera, B.K. Mishra, G.B. Behera, Chem. Rev. 100 (2000) 1973–2011.
[11] W. Sun, S. Guo, C. Hu, J. Fan, X. Peng, Chem. Rev. 116 (2016) 7768–7817.
[12] A. Sharma, P. Verwilst, M. Li, et al., Chem. Rev. 124 (2024) 2699–2804.
[13] J.L. Bricks, A.D. Kachkovskii, Y.L. Slominskii, et al., Dye. Pigment. 121 (2015) 238–255.
[14] Z. Lei, F. Zhang, Angew. Chem. Int. Ed. 60 (2021) 16294–16308.
[15] Z. Lei, C. Sun, P. Pei, et al., Angew. Chem. Int. Ed. 58 (2019) 8166–8171.
[16] R. Wei, Y. Dong, X. Wang, et al., J. Am. Chem. Soc. 145 (2023) 12013–12022.
[17] K.C.Y. Wong, E.M. Sletten, Curr. Opin. Chem. Biol. 68 (2022) 102131.
[18] Y. Yang, C. Sun, S. Wang, et al., Angew. Chem. Int. Ed. 61 (2022) e202117436.
[19] S. Pascal, S.H. Chi, J.W. Perry, C. Andraud, O. Maury, ChemPhysChem 21 (2020) 2536–2542.
[20] L.M. Tolbert, X. Zhao, J. Am. Chem. Soc. 119 (1997) 3253–3258.
[21] W. Xu, E. Leary, S. Sangtarash, et al., J. Am. Chem. Soc. 143 (2021) 20472–20481.
[22] M. Eskandari, J.C. Roldao, J. Cerezo, B. Milián-Medina, J. Gierschner, J. Am. Chem. Soc. 142 (2020) 2835–2843.
[23] P.A. Bouit, C. Aronica, L. Toupet, et al., J. Am. Chem. Soc. 132 (2010) 4328–4335.
[24] Y. Li, Y. Liu, Q. Li, et al., Chem. Sci. 11 (2020) 2621–2626.
[25] X. Ma, Y. Huang, S.A.A. Abedi, et al., CCS Chem. 4 (2022) 1961–1976.
[26] T. Furuyama, K. Satoh, T. Kushiya, N. Kobayashi, J. Am. Chem. Soc. 136 (2014) 765–776.
[27] J.P. Yang, R.H. Callender, J. Raman Spectrosc. 16 (1985) 319–321.
[28] K. Furuya, Y. Inagaki, H. Torii, Y. Furukawa, M. Tasumi, J. Phys. Chem. A 102 (1998) 8413–8421.
[29] D.L. Akins, S. Özçelik, H.R. Zhu, C. Guo, J. Phys. Chem. A 101 (1997) 3251–3259.
[30] J.T. Lopez Navarrete, G. Zerbi, J. Chem. Phys. 94 (1991) 957–964.
[31] C.M. McGoverin, T.J. Walsh, K.C. Gordon, A.J. Kay, A.D. Woolhouse, Chem. Phys. Lett. 443 (2007) 298–303.
[32] R. Andreu, E. Galán, J. Orduna, et al., Chem. Eur. J. 17 (2011) 826–838.
[33] Y. Yue, J. Ai, W. Chi, et al., Adv. Mater. 36 (2024) 2408450.
[34] V.G. Bandi, M.P. Luciano, M. Saccomano, et al., Nat. Methods 19 (2022) 353–358.
[35] M.J. Frisch, G.W. Trucks, H.B. Schlegel, et al., Gaussian 16, 2016.
[36] T. Lu, F. Chen, J. Comput. Chem. 33 (2012) 580–592.
[37] T. Lu, J. Chem. Phys. 161 (2024) 082503.
[38] R. Zhang, Z. Bi, L. Zhang, et al., ACS Nano 17 (2023) 19265–19274.
[39] Y. Liu, M. Gu, Q. Ding, et al., Angew. Chem. Int. Ed. 62 (2023) e202214875.